The Sixth International Workshop on Micro and Nanotechnology for Power Generation and Energy Conversion Applications, Nov. 29 - Dec. 1, 2006, Berkeley, U.S.A.

Performance of a High-Speed Microscale Turbocharger

N. Savoulides, S.A. Jacobson*, H. Li, C-J. Teo, J.M. Protz, A.H. Epstein

Massachusetts Institute of Technology – Gas Turbine Laboratory
Room 31-269, 77 Massachusetts Ave., Cambridge, MA 02139, U.S.A.
*Contact author: Phone: 617-253-2418, email: sjacob@mit.edu

Abstract

A MEMS turbocharger has been developed as part of an MIT program aimed at producing a microfabricated gas turbine engine for portable power applications. A gas turbine engine requires high-speed, high efficiency turbomachinery operating at tip speeds of several 100 m/s. This MEMS turbocharger serves to demonstrate these requirements. The turbocharger's silicon rotor, supported on hydrostatic gas thrust and journal bearings in a silicon stator housing, was spun to 480,000 rpm, corresponding to a tip speed of 200 m/s. This paper describes device operation and presents test results. The compressor demonstrated a pressure ratio of 1.21 at a mass flow rate of 0.13 g/s, at a combined compressor-turbine spool efficiency of 0.24. Under these conditions, the turbine produces about 5 W of power. Data are shown to compare well with analytical results.

Keywords: Micro power generation, Micro turbocharger, Micro gas turbine, Micro heat engine, PowerMEMS

1 - INTRODUCTION

As portable electronic devices proliferate, there is increased demand for improved compact power sources. Commercially available primary (non-rechargeable) batteries now provide energy densities upwards of 180 W-hr/kg, while secondary (rechargeable) batteries offer about 2/3 that level. Hydrocarbon fuels have a chemical energy density almost two orders of magnitude larger than current rechargeable batteries. So, a power source using hydrocarbon fuels with an electric power conversion efficiency of order 10% would be a revolutionary improvement. This promise has driven the development of the MIT micro gas turbine generator.

As the micro gas turbine generator is a complex system, its development has included several intermediate devices including the turbocharger described in this paper. The micro turbocharger serves to explore combined microscale turbomachinery fluid mechanics and rotordynamics, and to verify design models and analysis.

2 – DEVICE DESCRIPTION

Each turbocharger device is assembled from six 100 mm single-crystal silicon wafers that are typically etched on both sides to define features and then fusion bonded together. The multiwafer stack approach allows us to obtain three-dimensionality from a two-dimensional lithographic and etch process. The entire device requires over 20 different photomasks. Once bonded, the wafer stack is diced to form four separate devices as shown in Fig. 1.

The completed silicon turbocharger, measuring 23 mm x 23 mm x 2.9 mm, comprises a rotor and a stator housing as shown in cross-section in Fig. 2. The rotor is formed from wafer layers 3 and 4, and consists of a 6.0 mm diameter turbine etched into the bottom of layer 4 and an 8.2 mm diameter compressor etched into the top of layer 3. The turbocharger is geometrically the same as the gas turbine engine with the exception that the compressor discharge is not connected to the combustor inlet but rather exits the chip. Pressurized nitrogen supplied to the turbine inlet generates torque to spin the rotor, inducing mass flow and pressure rise through the compressor. Nitrogen is separately supplied to the hydrostatic gas thrust and journal bearings. A seal in line with the journal bearing isolates the compressor flow path from the turbine. The compressor exhaust is controlled by an external throttle valve, allowing variation of the compressor pressure ratio and mass flow rate.

Hydrostatic thrust bearings (TBs), centered on the front and aft faces of the rotor (Fig. 2), provide axial support. Twenty orifices supply a thin film of pressurized gas to the clearance gap separating the rotor from the static structure on the front and aft sides. The total axial clearance (front + aft) between

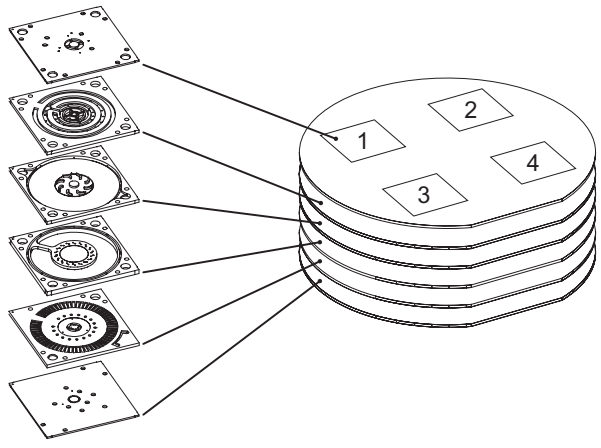

Figure 1 - The turbocharger is formed by fusion bonding six wafers to form four separate devices in the corners. The large die separation improves etch uniformity during the highly loaded blade etches.

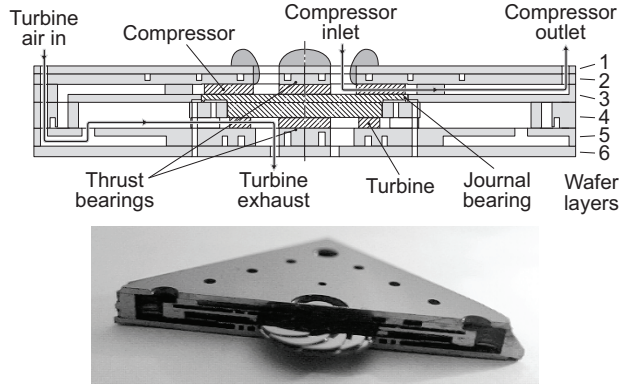

Figure 2 - Turbocharger cross-section. The hatched region in the top figure denotes the rotor.

the rotor and the static structure is 6 μm with a fabrication tolerance of ±0.25 μm. A hydrostatic journal bearing, located on the compressor rim, provides radial support. To ensure the rotor fits within the stator with the required tight thrust bearing clearance tolerance, the rotor is etched in place from the stator. The etch that frees the rotor also determines the journal bearing gap, located on the compressor rim. Dimensional control of the long, narrow journal bearing gap (depth 300 ±20 μm, width 16 ±0.5 μm) proved to be a major process challenge. High tolerance journal bearings were achieved through refinements in the etch recipe as well as modifications to the masking material profile [1]. With the current process, 60% of journal bearings meet specification. A more complete description of the bearing design can be found in references [2-6].

3 – EXPERIMENTAL SETUP

A gas handling system is used to control and monitor pressures and mass flow rates within the turbocharger. The compressor inlet was open to ambient. The compressor discharged to a throttle valve that was maintained at a fixed area during each test. After exiting the throttle, the flow passed through a mass flow meter and then exhausted to the room. Gas to the turbine was supplied via a mass flow controller. The turbine discharged through a throttle valve to a vacuum pump to permit the back pressure on the rotor to be adjusted to avoid excessive load on the thrust bearings. The back pressure was less than 20 kPa below atmospheric pressure.

Pressure regulators maintained steady supply pressure to the thrust bearings. Flow rate through a thrust bearing is primarily a function of differential pressure and geometry. During a test, both thrust bearings were held at fixed differential pressure. Turbine back pressure was adjusted to maintain a fixed flow rate to the thrust bearings, which enforces operation at a fixed axial position.

The rotor operation proved sensitive to the journal bearing differential pressure. Stable operation required fine pressure control, obtained by using a pressure regulator followed by a metering valve. The journal bearing flow and supply pressure were monitored at all times. Pressure taps within the turbocharger monitored turbine supply pressure, turbine inter-row pressure, turbine exhaust pressure, compressor inter-row pressure, and compressor exhaust pressure. A fiber-optic displacement sensor was used to measure the angular speed of the rotor. This sensor viewed six "speed bumps" located on the compressor just outside of the thrust bearing. The sensor's output was monitored on a spectrum analyzer.

The rotor dynamics of these devices presented an operational challenge since the operating speed is well above the natural or critical frequency of the journal bearing, requiring supercritical operation. Considerable effort was expended in learning how to safely cross the critical frequencies as the turbochargers accelerated to operating speed. The rotor is initially floated on the bearings and spun to a subcritical speed. While maintaining stable subcritical operation, the journal bearing differential pressure is lowered, which reduces the journal bearing damping ratio. The turbine inlet pressure is then quickly increased to accelerate the rotor through the critical frequency. Reducing the damping ratio effectively lowers the amplitude of the radial excursion as the rotor passes through the critical frequency [2].

With the rotor spinning supercritically, a rotordynamic map was used to follow a pre-specified speed/bearing pressure trajectory to reach higher speeds. The rotational frequency was maintained between the third and fourth integer multiples of the larger journal bearing natural frequency by increasing the bearing differential pressure (and thus its natural frequency) as the turbine speed was increased (Fig. 3). The bearing natural frequencies were measured in earlier tests, and shown to compare well with models [6]. The journal bearing has two close natural frequencies resulting from its asymmetric pressurization [5]. The trajectory was not strictly followed, but provided guidance during the acceleration phase. Experimentally, the rotor had stability issues at speeds that were less than two times the journal bearing natural frequency. The differential pressure across the journal bearing was limited to about 40 kPa to stay in a flow regime in which the bearing model assumptions are

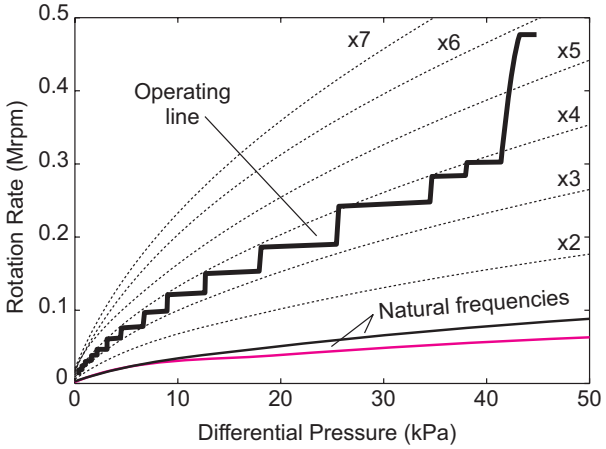

Figure 3 – Rotordynamic acceleration map for test 1. Operating schedule chosen to initially stay between the 3rd and 4th multiple of the larger natural frequency.

valid and to maintain a sufficient amount of damping ratio. The stability models predicted that the bearings should have been stable to over one million rpm at this pressure.

4 – EXPERIMENTAL RESULTS

Experiments were conducted with several devices [6]. Only the results obtained from the turbocharger that attained the highest speed are presented here. The geometry of this device is summarized in Table 1. Two tests were made at different, but fixed, compressor throttle areas. The rotor was spun to 480,000 rpm in the first test. The compressor throttle area was reduced for the second test, during which the rotor fatally crashed at a speed of 460,000 rpm. Data suggests that the crash was related to a tipping or coning motion of the rotor rather than a journal bearing instability. A coupled angular/translational dynamic model of the rotor and bearing system explained the cause for this coning motion [5]. Modifications to the internal bearing gas supply system have been designed to reduce coning motion in future devices.

Table 1: Geometry of the turbocharger tested

Parameter	As Built
Journal bearing length, clearance	291 μm, 17.4 μm
Seal length, clearance (centered)	200 μm, 7.5 μm
Forward TB nozzle length, diameter	108 μm, 9.0 μm
Aft TB nozzle length, diameter	111 μm, 9.3 μm
Total thrust bearing clearance	6.1 μm
Blade height: compressor, turbine	260 μm, 255 μm
Imbalance (offset of mass center from geometric center)	0.8 μm

Figure 4 shows the measurements of pressure ratio across the compressor and turbine. At 480,000 rpm the turbine was driven by a pressure ratio of 1.7 with a flow of 0.26 g/s to drive the compressor to a pressure ratio of 1.21 and a flow of 0.13 g/s. The compressor was designed to deliver a pressure ratio of 3:1 at 1.2 Mrpm, so these experimental results are off-design in a fluid mechanic sense. Compressor temperature ratio varies quadratically with rotational speed, and pressure ratio varies at a slightly higher power than this, assuming ideal gas relations. A functional fit to a design point 3-D CFD analysis is also plotted in Fig. 4, showing that the compressor measurements followed the expected functional form and the throttle area during the tests was close to the design point (within measurement uncertainty).

Figure 5 shows compressor and turbine pressure versus flow rate characteristics ("maps") based on measurements from the two tests. The compressor map includes only two points at each speed as each experiment was run at a fixed compressor throttle area. As is expected for a compressor, decreasing the compressor throttle area at fixed speed resulted in a mass flow increase and pressure ratio decrease. The turbine map is independent of the compressor-side throttle area as expected. Results from 3-D CFD compressor analyses at 287 krpm are also shown in Fig. 5. These analyses do not account for any pressure rise across the diffuser, which is not expected at these far off-design

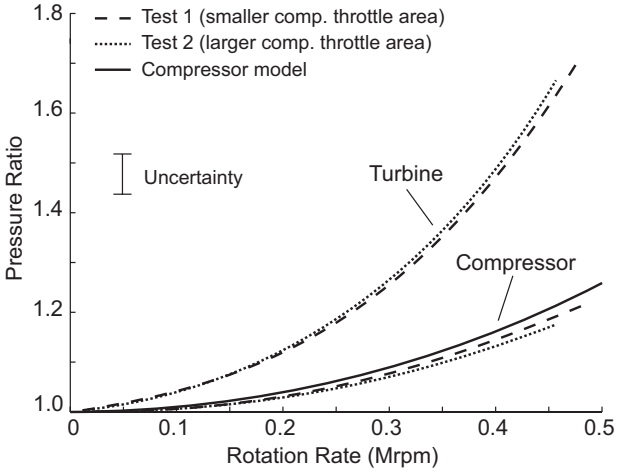

Figure 4 – Pressure ratios measured across the compressor and turbine.

operating conditions. Extrapolating the CFD data to the throttle area used during the experimental tests indicates the CFD is consistent with the measured test results within experimental uncertainty.

Measurements of the individual compressor and turbine efficiencies were not made due to the difficulty of making such measurements in non-adiabatic devices this small (which would require new experimental approaches). However, since the fluid enthalpy input to the turbine and the

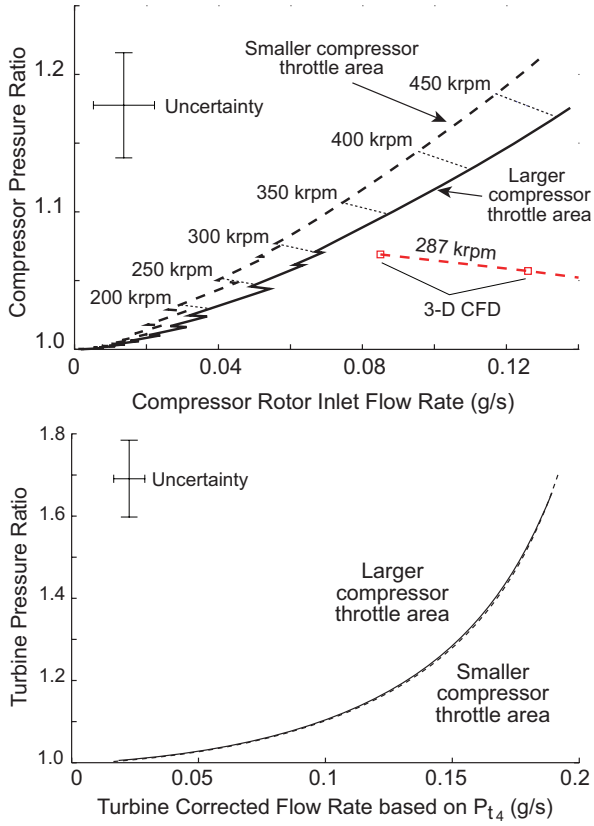

Figure 5 – Compressor map (top) and turbine map (bottom).

fluid power produced by the compressor were measured, the efficiency of the turbocharger as a whole is known. The losses in the machine consist of fluid losses in the compressor and turbine (which scale with mass flow) plus the parasitic mechanical losses in the bearings and seals (which scale with rotational speed). By modeling the parasitic losses, it was possible to determine the product of the compressor and turbine efficiencies based on the measurements. Figure 6 depicts the predicted parasitic losses as well as the ideal compressor and turbine isentropic power based on the measured pressure ratios. The powers in Fig. 6 clearly do not balance as the actual turbomachinery performance is far from ideal. A power balance can be written by introducing conventional efficiency factors:

$$\eta_t P_{ts} = \frac{P_{cs}}{\eta_c} + P_{loss} \qquad (1)$$

where η_t and η_c are the turbine and compressor isentropic efficiencies, P_{ts} and P_{cs} are the turbine and compressor isentropic powers, and P_{loss} represents the combined parasitic losses.

Inserting the measured and modeled values of Fig. 6 into Eq. (1) results in a functional relation between the compressor and turbine efficiencies at any given operating point. Figure 7 depicts this relation for several different rotating speeds. Note that these lines are a locus of possible combinations of turbine and compressor efficiencies. Only one point on each line can represent the actual values, however our available measurements were insufficient to determine this point. Figure 7 indicates that the turbomachinery performance is improving significantly with speed, as one would expect for components that are operating far off-design. Choosing points along the 480,000 rpm line shows that the product of the compressor and turbine efficiency is approximately 0.24. Three-dimensional CFD (Fluent) calculations of the compressor and turbine flows at 480,000 rpm resulted in efficiency values consistent with the measurements (Fig. 7). If the turbine and compressor efficiencies continue to increase with speed as the component CFD suggests, the engine model predicts that overall performance will be sufficient for a gas turbine cycle.

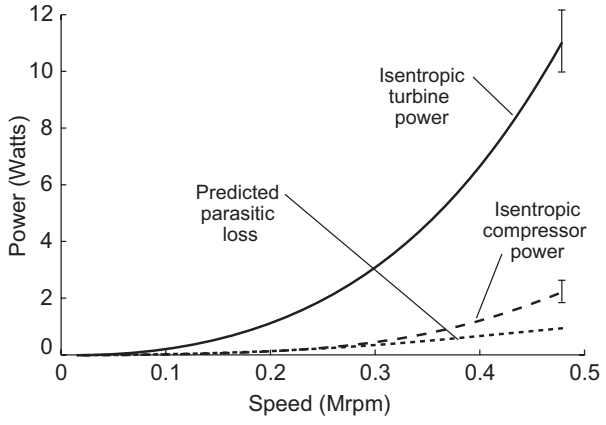

Figure 6 – Isentropic power to turbine and from compressor, and predicted parasitic loss.

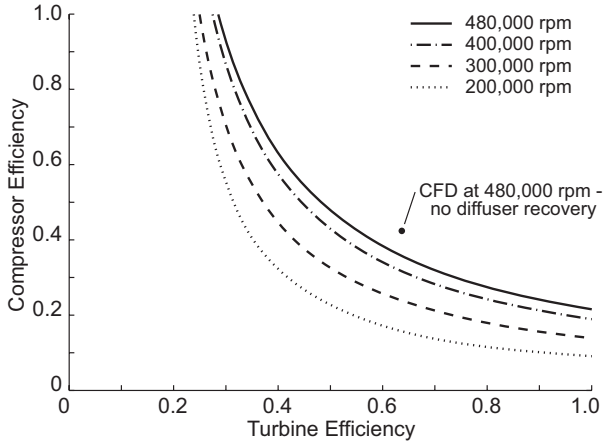

Figure 7 – Turbine/compressor efficiency relations based on measured spool performance and predicted parasitic losses.

5 - CONCLUSIONS

A silicon micro-turbocharger has been developed and tested. The compressor achieved a pressure ratio of 1.21 with a flow of 0.13 g/s at a tip speed of 200 m/s. The tip speed achieved is an order of magnitude faster than previously published work [7] and the pressure rise and flow rate are considerably higher than for any other silicon device we are aware of. The turbomachinery perform comparably to conventional scale components, and standard computational and analytic models appear to predict the flow accurately. Component efficiencies estimated from the experimental results are consistent with the values required to achieve closed cycle operation of a silicon MEMS gas turbine engine.

ACKNOWLEDGMENTS

This work was supported by the U.S. Army Research Laboratory. The authors thank L. Ho, L. Liu, Z. Spakovszky, F. Ehrich, M. Schmidt, J. Brisson, and Y-F Gong for their advice and assistance throughout this work.

REFERENCES

[1] Li, H., Savoulides, N., Ho, L., Jacobson, S.A., Khanna, R., Teo, C.-J., Wang, L., Ward, D., Epstein, A.H., and Schmidt, M.A., "Fabrication of a High Speed Microscale Turbocharger," *Hilton Head 2004*, Hilton Head Is., SC, 2004.

[2] Liu, L.X., Teo, C.J., Epstein, A.H., and Spakovszky, Z.S., "Hydrostatic Gas Journal Bearings for Micro-Turbomachinery", *J. Vibration and Acoustics*, Vol. 127, p. 157, April 2005.

[3] Teo, C.J., and Spakovszky, Z.S., "Modeling and Experimental Investigation of Micro-Hydrostatic Gas Thrust Bearings for Micro Turbomachines." Paper GT-2005-68222, *Proc. ASME TURBO EXPO 2005*, 2005.

[4] Teo, C.J., Spakovszky, Z.S., and Jacobson, S.A., "Unsteady Flow and Dynamic Behavior of Ultra-Short Lomakin Gas Bearings," *Proc. IJTC2006*, San Antonio, TX, October 2006.

[5] Liu, L., "Theory for Hydrostatic Gas Journal Bearings for MEMS," MIT PhD Thesis, September 2005.

[6] Savoulides, N., "Development of a MEMS Turbocharger and Gas Turbine Engine," MIT PhD Thesis, February 2004.

[7] Kang, P., Tanaka, S. and Esashi, M., "Demonstration of a MEMS-based turbocharger on a single rotor," *J. Micromech. Microeng*., Vol. 15, pp. 1076-1087, 2005.